Exchange bias and enhanced magnetoelectric effect in $FeNiMo_3O_8$

Junkai Yang,[1,2] Ying Meng,[1,2] Xiangfei Li,[1,2] Luyao Wang,[1,2] Haoyu Zhuang,[1,2] Jie Zhang,[1,2] Xi Shen,[1,*] Youwen Long,[1,2] and Richeng Yu[1,2,3,†]

[1]*Beijing National Laboratory for Condensed Matter Physics, Institute of Physics, Chinese Academy of Sciences, Beijing 100190, People's Republic of China*

[2]*School of Physical Sciences, University of Chinese Academy of Sciences, Beijing 100049, People's Republic of China*

[3]*Songshan Lake Materials Laboratory, Dongguan, Guangdong 523808, People's Republic of China*

(Received 25 September 2024; revised 1 June 2025; accepted 18 June 2025; published 7 July 2025)

Magnetoelectric (ME) materials face challenges in terms of practical applications and understanding of the underlying mechanisms of some phenomena. Studying these phenomena in glassy systems may provide fresh insights, but research along these lines remains limited. Our study reveals the existence of a glassy state at high temperature in single-crystal $FeNiMo_3O_8$ (FNMO), providing a unique perspective for comprehending other high-temperature physical phenomena in this system. Remarkably, FNMO exhibits enhanced ME coupling, achieving the ME effect at elevated temperatures relative to other members of the $M_2Mo_3O_8$ family, and coupling with a higher second-order ME coefficient than its parent phase. Our research establishes a direct relation between the ME effect and the glassy state. The emergence of exchange bias in FNMO is controlled by the spin coupling at the interface between the glassy state and the antiferromagnetic state, opening up novel pathways for developing high-performance magnetic memories by using single-phase materials.

DOI: 10.1103/yn33-jfp3

I. INTRODUCTION

In the broad field of condensed-matter physics and materials science, the magnetoelectric (ME) effect and exchange bias (EB) are of crucial importance due to their significance in advanced technological applications. The ME effect is observed in materials that exhibit an electrical response in magnetic field and vice versa. This phenomenon is pivotal in promoting innovative applications in fields such as information storage [1], sensors [2], and novel logic devices [3]. Likewise, EB, characterized by a noticeable shift in the magnetic hysteresis loop of certain systems, is crucial for enhancing the stability and performance of spin-based memories [4,5] and electronic devices [6].

Historically, the research in these fields has been focused mainly on materials with long-range magnetic order. In the field of ME, traditional multiferroics, which break inversion symmetry, have been extensively explored [7,8]. Although considerable progress has been made, its practical applications still face great challenges. For instance, type-I multiferroics exhibit weak ME effects [9], while type-II multiferroics require low operating temperatures to induce electric polarization [10], which limits their practical applications. These challenges highlight the necessity of finding novel methods for advanced ME materials. In the field of EB research, the main focus has been on magnetic heterostructures, particularly ferromagnet/antiferromagnet (FM/AFM) bilayers [11,12]. Nonetheless, after over 70 years of research, a thorough understanding of EB, especially regarding the influence of disorder and spin frustration at interfaces, remains an unresolved problem [13,14].

The spin-glass (SG) state is at the forefront of current research, playing a crucial role in revealing the complexities of ME and EB phenomena in new materials. Recent investigations demonstrated that long-range magnetic order is not a prerequisite for ME coupling in certain glassy systems [15]. More importantly, these materials reveal innovative ME coupling mechanisms [16] and demonstrate the potential for ME coupling at higher temperatures [17], thus opening up new avenues for research. Additionally, the EB phenomenon, traditionally observed in magnetic heterostructures, was identified in single-phase SG materials [18,19]. Those explorations into a glassy state indicate a promising direction for further understanding the underlying mechanisms of the ME effect and EB. The glassy state is characterized by disordered and metastable magnetic moments [20], which are in stark contrast to the ordered states in FM or AFM materials. The inherent frustration in glassy systems, stemming from structural disorder [21], chemical intermixing [22], or competing exchange interactions [23], is a critical aspect. Due to the fact that the intersection of a glassy state and the ME effect is a burgeoning field of research, examples of such systems are scarce, so targeted searches based on the magnetic cluster formation condition are both meaningful and necessary.

The $M_2Mo_3O_8$ (M = Mn, Fe, Co, Ni) family, which is well known for its intricate magnetic phase competition [24–28], provides an ideal framework for investigating these complex phenomena. Belonging to the polar space group $P6_3mc$ [29], its crystal structure features layers arranged in a honeycomb-like pattern for M_2 and a kagome-like structure for Mo_3 along

*Contact author: xshen@iphy.ac.cn
†Contact author: rcyu@iphy.ac.cn

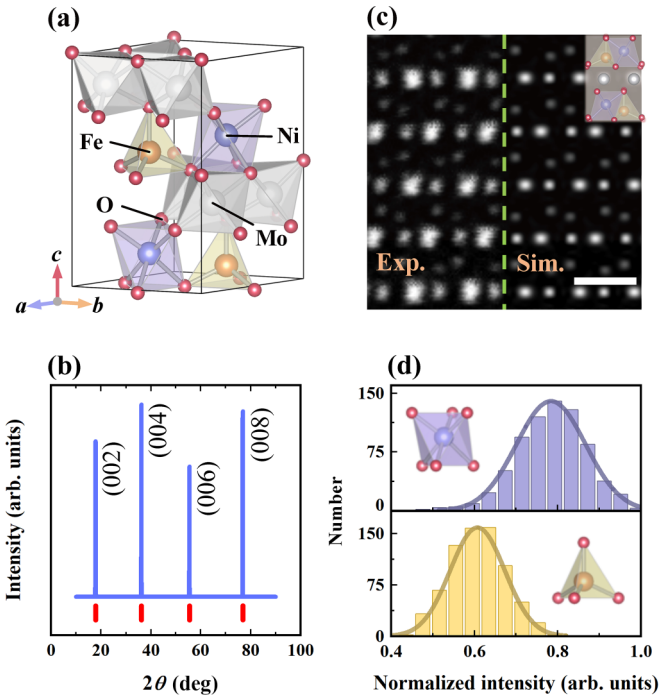

FIG. 1. Structural characterizations of FNMO. (a) Crystalline structure of FNMO. (b) XRD pattern of as-grown single crystal. (c) HAADF image of FNMO along the [100] direction, with a scale bar of 0.5 nm. The left side shows an experimental image, while the right side displays a simulated image. The parameters used for the simulation are based on those under real experimental conditions. The structural model overlaid on the upper right corner of the image represents Mo atoms as white spheres and O atoms as red spheres. Yellow and purple markings, respectively, indicate tetrahedral sites occupied by Fe atoms and octahedral sites occupied by Ni atoms. (d) The statistical results of the intensities for tetrahedral sites and octahedral sites in the experimental image, where the intensities are normalized. The yellow (purple) curve represents the Gaussian fitting result of the intensity distribution at tetrahedral (octahedral) sites.

the *c*-axis [Fig. 1(a)]. Despite $M_2Mo_3O_8$ exhibiting significant polarization and a pronounced ME effect, the operational temperature is typically below 60 K, posing a limitation for practical applications. Furthermore, the understanding of the $M_2Mo_3O_8$ family, especially at high temperatures, is still developing. Phenomena such as negative thermal expansion [30], the optical diode effect [31], and unusual phonon modes [32] highlight significant gaps in our knowledge. The rich magnetic phase competition in $M_2Mo_3O_8$ creates favorable conditions for the emergence of a glassy state. The potential existence of a glassy state could provide a new perspective for explaining these anomalies observed at high temperatures, thus requiring further experimental validation.

Inspired by these insights, we focus our attention on $FeNiMo_3O_8$ (FNMO), a material in the $M_2Mo_3O_8$ family that has not been extensively investigated before. In terms of structural analysis, the synthesized single-crystal samples provide reliable experimental evidence for settling the long-standing debate about atom occupation. The results indicate that Ni^{2+} ions tend to occupy octahedral sites. Regarding the physical properties, various experimental approaches consistently indicate the existence of a glassy state in FNMO at higher temperatures ($T < 125$ K), providing a reasonable explanation for the concurrent negative thermal expansion phenomenon. Furthermore, at lower temperatures ($T < 50$ K), FNMO exhibits both an AFM state and a glassy state. The interaction between these two magnetic phases leads to the emergence of EB. Notably, FNMO exhibits a significant enhancement in ME coupling, achieving the ME effect at higher temperatures than other members of the $M_2Mo_3O_8$ family and displaying a substantial increase in the second-order ME coefficient with respect to the parent phase $Fe_2Mo_3O_8$. Additionally, our experiments demonstrate a significant correlation between the ME effect and the glassy state in FNMO. This research aims not only to bridge the gaps in our understanding of these complex magnetic phenomena, but also to lay a foundation for developing high-performance magnetic memories and high-temperature ME applications.

II. MATERIALS AND METHODS

Single crystals of FNMO were successfully synthesized using the chemical vapor transport reaction, as detailed in Ref. [33]. We utilized high-purity materials, including Fe, Fe_2O_3, NiO, and MoO_2, along with $TeCl_4$ as a transporting agent. These components were sealed in evacuated silica tubes and then subjected to a two-zone furnace process at 1000 °C for a duration of 10 days, facilitating crystal growth. The compositional analysis was conducted using scanning electron microscopy (SEM) (HITACHI, Regulus 8230) paired with energy-dispersive x-ray (EDX) spectroscopy. X-ray diffraction data were collected using a diffractometer (Bruker, D8 VENTURE), utilizing Mo $K\alpha$ radiation ($\lambda = 0.710\,73$ Å) at a temperature of 293(2) K. For structural refinement, we employed the SHELXL software package [34]. Specimen preparation for scanning transmission electron microscopy (STEM) was carried out using focused ion beam milling (FEI, Helios 600i). The atomic structure was subsequently examined with a transmission electron microscope (JEOL, ARM 300F), which features double spherical aberration correctors, achieving a spatial resolution below 63 pm at 300 kV. A multiline simulation program (HREM Research, xHREM) was utilized for the quantitative analysis of the STEM image [35].

For the measurement of dc molar susceptibility (χ_m) and magnetization (M), we employed a magnetic property measurement system (Quantum Design, MPMS-3). The ac molar susceptibility and electrical properties were assessed using a physical property measurement system (Quantum Design, PPMS-9T). To measure the relative dielectric constant (ε_r) and electric polarization (P), silver paste electrodes were applied to the parallel end surfaces of the specimen. The ε_r were determined at various frequencies using an LCR meter (Agilent, E4980A). The value of P was calculated by integrating the time of the polarization current, recorded with a precise electrometer (Keithley, 6517B). For pyroelectric current (J) measurements, the sample underwent cooling from 200 to 5 K with a poling electric field ($E_{pol} = \pm 480$ kV m^{-1}). J was recorded from 5 to 150 K post removal of E_{pol} and a subsequent 30-min wait to dissipate space charges, thereby mitigating any extrinsic contributions. The ε_r and J measurements, responsive to temperature and magnetic field, were

performed at a warming rate of 2 K min^{-1} and a magnetic field ramping at 100 Oe s^{-1}.

III. RESULTS AND DISCUSSION

The FNMO single crystal generally exhibits the characteristics of a hexagonal prism, which is consistent with sixfold rotational symmetry. We quantitatively analyzed the elemental composition in different regions of the sample by using an energy-dispersive spectrometry (EDS), and the results are shown in Table S1 of the Supplemental Material [36]. The elemental ratios in different regions of the sample are almost the same, with the average result showing Fe : Ni = 0.48 : 0.52 and (Fe + Ni) : Mo = 2.03 : 3, which are essentially consistent with the nominal composition ratios. To confirm the symmetry of the sample, we characterized the crystal structure in detail by using x-ray diffraction (XRD) and selected-area electron diffraction (SAED), and the results are shown in Figs. 1(b) and S1, respectively [36]. The sharp and clear diffraction peaks, along with the diffraction pattern that possesses the same characteristics as $Fe_2Mo_3O_8$, indicate that the sample has the space group $P6_3mc$ and good crystallinity.

In previous studies on FNMO polycrystals [37,38], the specific occupancy of Fe and Ni in the crystal structure is still a contentious issue. Due to our successfully growing FNMO single-crystal samples, we have an opportunity to investigate this issue in greater depth. To obtain a more accurate understanding of the occupancy rate of doping atoms, we refined the structure of single-crystal XRD (SCXRD) data as listed in Table S2 [36]. The refinement result shows that a weighted R-factor wR_2 is only 3.36%, highlighting the high reliability of the research results [39]. The lattice constant of FNMO is between those of $Fe_2Mo_3O_8$ and $Ni_2Mo_3O_8$. The Ni content is determined to be approximately 51%, which is consistent with the EDS data. More importantly, the refinement also reveals that the octahedral positions are almost entirely occupied by Ni^{2+} ions (see Table S3 [36]), which is consistent with Mössbauer spectroscopy observations [37].

Furthermore, we conducted a more in-depth study of the crystal structure by using scanning transmission electron microscopy (STEM). The left half of Fig. 1(c) displays a high-angle annular dark-field (HAADF) image of FNMO along the [100] direction. The statistical analyses for the intensities of atoms at tetrahedral and octahedral positions in the image are shown in Fig. 1(d). The intensities at both positions follow a normal distribution, and it is noteworthy that the intensity at the octahedral position is significantly higher than that at the tetrahedral position. This is also consistent with the conclusion we obtained previously through the refinement of SCXRD. The higher intensity at the octahedral position is due to the larger atomic number of Ni than that of Fe [40,41]. To verify the accuracy of the statistical result, we constructed two different occupancy structure models and validated them by using HAADF image simulation. From the simulation results, the structure model with Ni^{2+} ions at the octahedral positions is more consistent with the experimental result (see Fig. S2 [36]). Taking into consideration both the refinement results of the SCXRD and the intensity statistics of the HAADF images, we can conclude that in FNMO, Fe^{2+} ions are more inclined to occupy tetrahedral positions, while Ni^{2+} ions tend to encroach on octahedral positions.

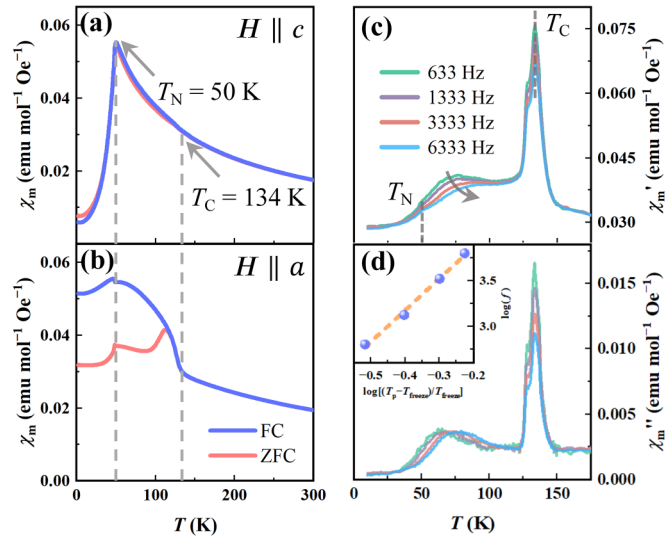

FIG. 2. Temperature-dependent magnetic susceptibility of FNMO. Variations of dc molar susceptibility χ_m with temperature along (a) the c-axis and (b) the a-axis, where the FC and ZFC data are represented by a blue line and a red line, respectively. The gray dashed lines denote the Curie transition temperature T_C in panel (a) and the Néel transition temperature T_N in panel (b). (c) Variations of real part χ'_m and (d) imaginary part χ''_m of ac susceptibility with temperature along the a-axis. The data are measured at different frequencies and an amplitude of 10 Oe. The inset in panel (d) shows the plot of $\log(f)$ vs $\log[(T_p - T_{freeze})/T_{freeze}]$ and the best fit (orange dashed line).

We also measured the lattice constants of FNMO at varying temperatures by using SAED. Figure S3 shows SAED patterns taken at room temperature and in a liquid nitrogen temperature region [36]. After cooling, no new diffraction spots are observed and the diffraction pattern remains unchanged, indicating that FNMO does not undergo a structural transition at 95 K. The analysis of the lattice constants reveals an increase in the lattice parameters of FNMO after cooling, as shown in Table S4 [36]. Similar negative thermal expansion phenomena were observed in both $Fe_2Mo_3O_8$ and $Ni_2Mo_3O_8$ [38], and neutron powder diffraction indicated that the negative expansion may be related to short-range magnetic order [42]. Therefore, we subsequently conducted an in-depth study of the magnetic properties of FNMO.

Figures 2(a) and 2(b) show the temperature-dependent magnetic susceptibility obtained when 0.1 T is applied along the c-axis and a-axis, respectively. The χ_m of FNMO along the c-axis exhibits distinct AFM characteristics, specifically, it begins to decline at the onset temperature of the Néel transition ($T_N = 50$ K) and approaches zero at low temperatures. The similarity of the susceptibility curves with those of $Fe_2Mo_3O_8$ suggests that the spins in FNMO are likely aligned along the c-axis. Interestingly, in the results obtained along the a-axis, the χ_m shows not only a small peak at T_N, but also a characteristic similar to a ferrimagnetic (FIM) transition at a higher temperature ($T_C = 134$ K). As a function of temperature, the magnetization of FNMO at high temperatures ($T > 150$ K)

follows the Curie-Weiss law (Fig. S4 [36]):

$$\chi_m(T) = \chi_0 + \frac{C}{T-\theta}, \tag{1}$$

where χ_0 represents the temperature-independent contribution. The values of Curie-Weiss temperature θ for both directions are negative, specifically, $\theta_c = -64\,\mathrm{K}$ and $\theta_a = -178\,\mathrm{K}$, indicating that the spin coupling in the material exhibits AFM characteristics. Further comparison between the magnetic moments $\mu_c = 3.40\mu_B$ and $\mu_a = 4.18\mu_B$, which are derived from Curie constant C, indicates significant magnetic anisotropy between the *ab* plane and the *c*-axis. Due to the orbital-driven Peierls effect, Mo^{4+} ions form nonmagnetic trimers [43,44]. This results in only Fe^{2+} (with a theoretical spin value of only $4.90\mu_B$) [45] and Ni^{2+} ($2.83\mu_B$) ions contributing to magnetism in FNMO. The FNMO displays a more complex magnetic structure than $Fe_2Mo_3O_8$, and a higher magnetic ordering temperature than $Ni_2Mo_3O_8$. Its changes stem from the preferences of Ni and Fe ions for a unique site. In magnetic materials, the preference for a specific crystallographic site significantly influences the exchange interaction that is crucial for establishing magnetic order. The intricate interaction dynamics between the Fe and Ni ions in FNMO may also explain the observed FIM-like transition at higher temperatures than in the parent phase.

It is noteworthy that both the field-cooling (FC) curve and the zero-field-cooling (ZFC) curve bifurcate when the temperature is lower than T_C, which indicates that the irreversibility occurs in different cooling processes. This kind of bifurcation phenomenon was reported in glassy materials and superparamagnetic systems [46,47]. To understand the nature of this phenomenon, we measured the real part χ'_m and imaginary part χ''_m of the alternating current (ac) molar susceptibility of FNMO, and the results are shown in Figs. 2(c) and 2(d). First, a frequency-independent peak is observed at T_C in each curve, which is a characteristic of FIM order [48]. Second, a small anomaly is observed just below 134 K, meaning the onset of a transitional magnetic state, arising from competing magnetic phases in the frustrated FNMO. Third, as the temperature decreases, a pronounced frequency-dispersive bulge appears in χ'_m. The peak position, T_p, shifts with the change of applied frequency, indicating the existence of a glassy state in the material. These peaks, which represent the FIM state, the transitional magnetic state, and the glassy state transition, respectively, are also observed in χ''_m. The relationship of T_p with frequency can be described by using a dynamic scaling law [49,50]:

$$\tau = \frac{1}{2\pi f} = \tau_0\left(\frac{T_p - T_{freeze}}{T_{freeze}}\right)^{-zv}, \tag{2}$$

where τ_0 is related to the characteristic spin flipping time, zv is the dynamic critical exponent, and T_{freeze} is the static freezing temperature for the glassy state. The fitting result indicates that T_{freeze} is about 49 K as indicated in the inset of Fig. 2(d). Notably, for a canonical SG system the τ_0 lies between $\sim 10^{-12}$ and 10^{-13} s [48,51,52], which is smaller than the observed value of 10^{-6} s by a few orders. The larger τ_0 indicates toward freezing of magnetic clusters [53].

Previous studies show that a multivalley energy landscape generated by spin frustration occurs after the material has

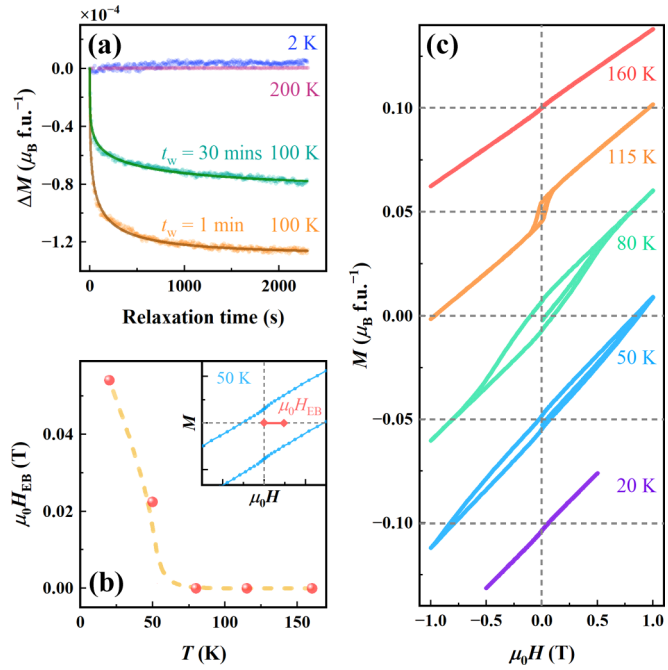

FIG. 3. Glassy state characterization and exchange bias of FNMO. (a) Thermoremanent magnetization measurements (dots) along the *a*-axis performed at various temperatures with corresponding fits (lines). The sample is cooled to the target temperature in a field of 0.1 T along the *a*-axis, and after a period t_w, the magnetic field is removed and the relaxations are recorded. (b) Temperature-dependent exchange bias field $\mu_0 H_{EB}$, which is extracted from each loop by taking the average of the x intercepts. The inset shows the definition of $\mu_0 H_{EB}$ (red line). (c) Hysteresis loops along the *a*-axis at different temperatures, with the dashed lines marking the position of the origin. Data are vertically shifted for clarity. Under each test condition, the sample is first heated to the paramagnetic state (200 K) and then cooled to the target temperature in zero field so as to eliminate the interference of the residual magnetization in the sample with the experimental results.

entered the glassy state [20,46,54]. This nonergodic nature leads to complex magnetic relaxation process, manifested as slow variation in magnetization over time after the external magnetic field has been removed. For the measurement of thermoremanent magnetization (TRM), the sample needs to be cooled to the target temperature under an applied magnetic field, then maintained for a period t_w under that applied field. These experimental results under different conditions are shown in Fig. 3(a). Notably, the magnetization does not show any relaxation phenomenon at 200 K nor 2 K, which is because at 200 K the material has not yet entered the glassy state, while at 2 K ($T < T_N$) the glassy state is frozen, which is consistent with the fitting result of $T_{freeze} \approx T_N$ obtained from Eq. (2). At 100 K, FNMO exhibits a relaxation phenomenon of magnetization over time, and this process can be described by using a typical stretched exponential decay function [55]:

$$M(t) = M_0 + M_G \exp\left[-\left(\frac{t}{t_0}\right)^{\beta}\right], \tag{3}$$

where M_0 represents the initial remnant magnetization, M_G is the magnetization of the glassy state component, t_0 is the

characteristic relaxation time constant, and β is the stretching exponent. The β values obtained for different values of t_w are 0.35 (orange line) and 0.25 (green line), respectively. Both of these fitted values are within the typical range for glassy systems [51,52,56]. Furthermore, longer t_w values are related to higher magnetization values, which is another characteristic feature of glassy magnetic systems [20,46].

The magnetization of the sample as a function of applied magnetic field is measured after ZFC, and the results are shown in Fig. 3(c). These two interesting characteristics are worth noting. First, it can be clearly seen that with the decrease of temperature, the hysteresis loop first appears and then disappears. These characteristic changes are the same as the behaviors of relaxation phenomena discussed previously, and the appearance temperatures of both phenomena ($T_N < T < T_C$) are the same, which further indicates that the uncompensated magnetic moment in the material originates from the glassy state. Second, when $T \leqslant T_N$, the hysteresis loop has a lateral shift, which is a characteristic of the EB [57,58]. The magnitude of the EB field, $\mu_0 H_{EB}$, can be calculated from the following formula:

$$\mu_0 H_{EB} = \frac{\mu_0 H_{int1} + \mu_0 H_{int2}}{2}, \tag{4}$$

where $\mu_0 H_{int1}$ and $\mu_0 H_{int2}$ are the intercepts on the horizontal axis as shown in the inset of Fig. 3(b). It can be noted that a distinct $\mu_0 H_{EB}$ appears as FNMO enters the AFM state, and $\mu_0 H_{EB}$ gradually increases with further decreasing temperature.

In the study of electrical properties of FNMO, we first characterized the variation of the relative dielectric constant ε_r with temperature, which is shown in Fig. 4(a). At the temperature of the AFM transition, anomalies are observed in ε_r along both the [001] and [120] directions, indicating that the magnetic phase transition in FNMO significantly affects its dielectric properties. In addition, the anomalies of the curve do not shift with frequency, thus ruling out the possibility of relaxor ferroelectricity. Unlike traditional ferroelectric material where ε_r exhibits a sharp peak at the phase transition, the change in ε_r of FNMO is relatively gradual, suggesting that FNMO may not possess ferroelectricity at low temperatures.

In the absence of an applied polarization electric field, we measured the pyroelectric current $J(T)$ of FNMO, and the results are represented by the dark green curve in Fig. 4(b). Several key points in the figure are noteworthy. First, the $J(T)$ signal appears in FNMO below 125 K, which coincides with the temperature of the glassy state identified through magnetic characterization, indicating a clear correlation between the two phenomena. Second, at the AFM transition temperature, $J(T)$ undergoes significant changes, indicating that long-range magnetic ordering triggers off an additional pyroelectric current. Lastly, a reverse $J(T)$ signal was detected at low temperatures ($\sim$ 30 K). Since the appearance of this signal does not coincide with any dielectric or magnetic anomalies, we believe that this is not intrinsic to the sample; the data below 30 K are shown for completeness only. Similar phenomena were observed in $J(T)$ measurements for other materials [59,60], but they are more likely to be due to the influence of free charges that are inevitable in the testing process [61,62].

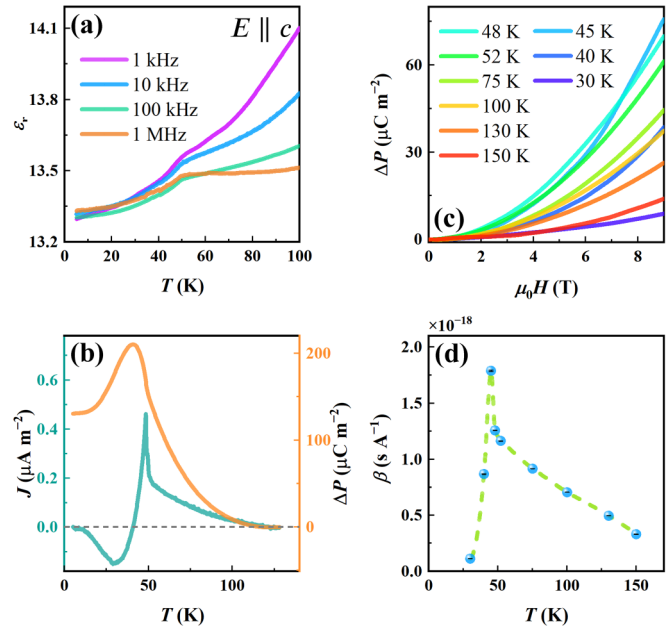

FIG. 4. ME coupling of FNMO. (a) Temperature-dependent relative dielectric constants under applied electric fields at four different frequencies. (b) Temperature-dependent pyroelectric current $J(T)$ (dark green curve) and electric polarization $\Delta P(T)$ (orange curve) along the c-axis. (c) Magnetic-field-dependent change of electric polarization $\Delta P(H)$ with $\mu_0 H(T)$ applied along the c-axis at various temperatures. (d) The second-order ME coefficients from the fitting as a function of temperature, with short black lines representing error bars.

By integrating $J(T)$ over time, we obtained the variation of the polarization $\Delta P(T)$ in FNMO as shown by the orange curve in Fig. 4(b). Like the trend of $J(T)$, $\Delta P(T)$ gradually strengthens with the emergence of the glassy state and peaks after the AFM transition, followed by a decrease due to the influence of free charges. Notably, this change in polarization does not reverse with the direction of the applied electric field changing (Fig. S5 [36]), indicating that FNMO exhibits pyroelectricity rather than ferroelectricity. Although the structure of FNMO belongs to a polar point group ($6mm$), its polarization direction cannot be switched. From an energy perspective, the opposite polarization states in ferroelectric materials typically have low-energy barriers, allowing for polarization reversal by applying electric fields similar to energy levels. However, in pyroelectric materials such as Ni_3TeO_6 [63] and $CaBaCo_4O_7$ [64], due to the asymmetry of the structure in the two polarization states, the energy barrier for reversing polarization is actually infinite.

Figure 4(c) shows the changes in polarization of FNMO under different magnetic fields, i.e., the ME effect. Notably, the ME coupling exhibits a trend of first increasing and then decreasing with decreasing temperature. To quantitatively analyze the ME effect, we use a second-order polynomial to fit the $\Delta P(H)$ curve and obtain the ME coefficient from

$$\Delta P = P_0 + \alpha H + \beta H^2, \tag{5}$$

where P_0 is the crystallographic and spin-induced spontaneous polarization, and α and β are the first-order and second-order

ME coefficient, respectively [24]. The fitting results indicate that the ME effect in FNMO mainly arises from β as shown in Fig. 4(d). With the emergence of the glassy state, the ME coefficient gradually increases with decreasing temperature but rapidly decreases below the AFM transition temperature. The magnitude of the ME coefficient in FNMO was analyzed, and the largest β was measured at 45 K (1.8×10^{-18} s/A), which has a significant enhancement of about ten orders of magnitude compared with the β at 45 K in $Fe_2Mo_3O_8$ (1.81×10^{-28} s/A) [65]. Additionally, compared with 1.7 K at which the β value in $Ni_2Mo_3O_8$ reaches -5.1×10^{-18} s/A [27], the temperature for ME coupling in FNMO is notably high.

The refinement result of SCXRD and the intensity statistics of HAADF images both indicate that in FNMO, Fe^{2+} ions tend to occupy tetrahedral sites, while Ni^{2+} ions are more inclined to encroach on octahedral sites. This preferential occupation can be analyzed from the perspective of ligand field theory. Ligand field stabilization energy (LFSE) represents the decrease in total energy of transition-metal d electrons entering the split energy levels formed by the crystal field, compared with entering into the degenerate state [45]. The difference in LFSE between octahedral complex and tetrahedral complex, ($LFSE_O$-$LFSE_T$), also known as octahedral site preference energy (OSPE), can quantitatively evaluate the degree of preference of different electronic configurations for ligand environments [66]. As shown in Table S5, the OSPE of the d^8 electronic state is smaller, indicating that Ni^{2+} ions preferentially occupy octahedral sites, thereby lowering the overall energy of the system [36,67]. This theoretical analysis provides a reasonable explanation for the experimental results of SCXRD and HAADF.

Multiple experimental methods confirm the existence of a glassy state in FNMO. First, the direct current (dc) magnetization curves show that below T_C, a bifurcation occurs between the FC curve and the ZFC curve, as can be seen in Figs. 2(a) and 2(b), which is typically attributed to the freezing of magnetic moments [68]. When the crystalline anisotropy of small domains overcomes thermal fluctuations, spins are frozen in random directions, leading the ergodicity to break down [69]. Varying the magnitude of the magnetic field applied in the measurement process can change the free-energy minimum value, thus causing a change in the temperature at which the FC and ZFC curves bifurcate as shown in Fig. S6 [36]. Second, the ac susceptibility curves exhibit two peaks, which represent the FIM state transition and the glassy state transition, respectively [Figs. 2(c) and 2(d)]. This characteristic of transitioning from long-range magnetic order to disordered phase after cooling is reminiscent of reentrant spin glass (RSG) [70]. Third, the measurements of magnetization over time reveal slow spin relaxation dynamics in FNMO [Fig. 3(a)], another characteristic feature of glassy magnetic materials. The formation of a glassy state is generally accompanied by disorder and frustration [71]. The FNMO crystallizes in the polar space group $P6_3mc$, featuring a honeycomb network for the M_2 layer. This two-dimensional lattice inherently contains triangular motifs, which prevent all nearest-neighbor spin couplings from simultaneously satisfying their lowest-energy configurations, thereby inducing geometric frustration. In $Fe_2Mo_3O_8$ and $Ni_2Mo_3O_8$, magnetic phase competition can be jointly controlled by magnetic field and temperature, thereby producing a variety of magnetic phases [27,65]. Additionally, the competing magnetic interactions within the system may lead to spin frustration, which hinders the formation of a perfectly ordered state, resulting in the emergence of a disordered phase [72].

The glassy state in FNMO generates a series of novel phenomena, such as the observation of EB below T_N [Fig. 3(b)]. Figure S6 shows that the FC and ZFC curves under 1 T field are virtually identical, demonstrating that the 1 T applied field is sufficient to overcome any remanent magnetization in the MPMS, thus eliminating its influence on the EB measurement [36]. Regarding the physical origin of the EB, the interaction between two magnetic phases is often considered to be a key factor in multilayer films [73]. Therefore, it can reasonably be expected that the coexistence of a glassy state and an AFM state in a single-phase material would also lead to the emergence of EB [19,74]. This implies that the pinning effect can exist not only at thin-film interfaces but also throughout the entire sample space. As the temperature decreases, the influence of thermal disturbances on the pinning effect weakens, causing $\mu_0 H_{EB}$ to increase rapidly. More importantly, like some RSG systems [74–77], EB can be observed after ZFC in FNMO, which is undoubtedly beneficial for the applications of EB in spintronic devices.

The ME effect in FNMO also shows a profound connection with the glassy state. A key observation is that the onset temperature of the pyroelectric current aligns with the formation temperature of the glassy state, both occurring around 125 K. This temperature is notably higher than those observed in other $M_2Mo_3O_8$ family members [24–27], including $Ni_2Mo_3O_8$ (5 K), $Co_2Mo_3O_8$ (40.5 K), $Mn_2Mo_3O_8$ (41.5 K), and $Fe_2Mo_3O_8$ (60 K), and also higher than those in some SG materials [16,78,15], such as $NiMnTiO_3$ (10 K), $SrMnTiO_3$ (38 K), and $BaCo_6Ti_6O_{19}$ (50 K), highlighting the distinctiveness of FNMO. In exploring the ME effect mechanism, previous investigations on $M_2Mo_3O_8$ mainly concentrated on long-range magnetic order, while our study reveals that short-range magnetic order can equally induce the ME effect. In FNMO, the significant spin-lattice coupling, inferred from the negative thermal expansion in the glassy state, likely contributes to this ME coupling [30,79]. Moreover, our quantitative analysis of the ME effect demonstrates that the ME coefficient first increases and then rapidly decreases as the temperature decreases [Fig. 4(d)]. This behavior in the high-temperature range ($T_N < T < T_C$) can be understood because decreasing temperatures cause the magnetic domain size to increase, thereby amplifying the ME effect in FNMO. However, when entering the AFM state ($T \leqslant T_N$), the interplay between the magnetic clusters and AFM phases cannot be ignored. The EB confirms the persistence of the glassy state, but the response of the magnetic clusters is markedly reduced by the influence of interfacial spin coupling. This interaction leads the ME coupling to decrease significantly, thereby providing a comprehensive explanation for the observed temperature-dependent behavior of the ME effect in FNMO.

IV. CONCLUSION

We have successfully synthesized single-crystal FNMO and conducted comprehensive studies on its structure,

magnetism, EB, and ME effect. Through SCXRD refinement and HAADF image contrast statistical analysis, it is confirmed that Ni^{2+} ions prefer to occupy octahedral sites. The existence of a glassy state in FNMO at high temperatures, caused by competing magnetic interactions, is confirmed through ac magnetic susceptibility and TRM measurements. The confirmation of the glassy state provides a new direction for explaining other novel physical phenomena occurring in this system at high temperatures. Notably, FNMO exhibits a significant enhancement in ME coupling. FNMO not only achieves the ME effect at higher temperatures than other members of the $M_2Mo_3O_8$ family, but it also shows a significant increase in the second-order ME coefficient, by 10 orders of magnitude compared with the parent phase $Fe_2Mo_3O_8$. Further research finds a close relation between the ME effect and the glassy state in FNMO, specifically, as the magnetic domains increase (or freeze), the ME coefficient correspondingly increases (or decreases). This discovery provides a new perspective for understanding the complex ME mechanisms in this family. After forming long-range magnetic order, the spin coupling at the interface between the glassy state and the AFM state leads to EB. The discovery of EB in this material provides a new approach for developing high-performance magnetic memories in single-phase materials. Overall, these research findings not only deepen our understanding of the magnetic structure and ME effect in $M_2Mo_3O_8$, but they also reveal that appropriate chemical doping can optimize its ME coupling performance, thus providing feasibility for the practical application of high-temperature ME.

ACKNOWLEDGMENTS

This work was supported by the National Key Research Program of China (Grants No. 2022YFA1402801 and No. 2024YFA1408000), the National Natural Science Foundation of China (Grants No. 12374132, No. 11874413, No. 11934017, and No. 51972333), and the Strategic Priority Research Program of the Chinese Academy of Sciences (CAS) (Grant No. XDB33030200).

[1] F. Zavaliche, T. Zhao, H. Zheng, F. Straub, M. P. Cruz, P.-L. Yang, D. Hao, and R. Ramesh, Electrically assisted magnetic recording in multiferroic nanostructures, Nano Lett. **7**, 1586 (2007).

[2] C. Israel, N. D. Mathur, and J. F. Scott, A one-cent room-temperature magnetoelectric sensor, Nat. Mater. **7**, 93 (2008).

[3] S. Manipatruni, D. E. Nikonov, C.-C. Lin, T. A. Gosavi, H. Liu, B. Prasad, Y.-L. Huang, E. Bonturim, R. Ramesh, and I. A. Young, Scalable energy-efficient magnetoelectric spin–orbit logic, Nature (London) **565**, 7737 (2019).

[4] S. Gider, B.-U. Runge, A. C. Marley, and S. S. P. Parkin, The magnetic stability of spin-dependent tunneling devices, Science **281**, 797 (1998).

[5] V. Skumryev, S. Stoyanov, Y. Zhang, G. Hadjipanayis, D. Givord, and J. Nogués, Beating the superparamagnetic limit with exchange bias, Nature (London) **423**, 6942 (2003).

[6] X. He, Y. Wang, N. Wu, A. N. Caruso, E. Vescovo, K. D. Belashchenko, P. A. Dowben, and C. Binek, Robust isothermal electric control of exchange bias at room temperature, Nat. Mater. **9**, 579 (2010).

[7] S. Dong, J.-M. Liu, S.-W. Cheong, and Z. Ren, Multiferroic materials and magnetoelectric physics: Symmetry, entanglement, excitation, and topology, Adv. Phys. **64**, 519 (2015).

[8] M. Fiebig, T. Lottermoser, D. Meier, and M. Trassin, The evolution of multiferroics, Nat. Rev. Mater. **1**, 16046 (2016).

[9] Y. F. Popov, A. K. Zvezdin, G. P. Vorob'ev, A. M. Kadomtseva, V. A. Murashev, and D. N. Rakov, Linear magnetoelectric effect and phase transitions in bismuth ferrite, $BiFeO_3$, JETP Lett. **57**, 69 (1993).

[10] C. Lu, M. Wu, L. Lin, and J.-M. Liu, Single-phase multiferroics: New materials, phenomena, and physics, Natl. Sci. Rev. **6**, 653 (2019).

[11] N. C. Koon, Calculations of exchange bias in thin films with ferromagnetic/antiferromagnetic interfaces, Phys. Rev. Lett. **78**, 4865 (1997).

[12] T. C. Schulthess and W. H. Butler, Consequences of spin-flop coupling in exchange biased films, Phys. Rev. Lett. **81**, 4516 (1998).

[13] K. Takano, R. H. Kodama, A. E. Berkowitz, W. Cao, and G. Thomas, Interfacial uncompensated antiferromagnetic spins: Role in unidirectional anisotropy in polycrystalline $Ni_{81}Fe_{19}$/CoO bilayers, Phys. Rev. Lett. **79**, 1130 (1997).

[14] H. Ohldag, A. Scholl, F. Nolting, E. Arenholz, S. Maat, A. T. Young, M. Carey, and J. Stöhr, Correlation between exchange bias and pinned interfacial spins, Phys. Rev. Lett. **91**, 017203 (2003).

[15] H. Tonomoto, K. Kimura, and T. Kimura, Magnetoelectric glass nature in magnetoplumbite-type $BaCo_6Ti_6O_{19}$, J. Phys. Soc. Jpn. **85**, 033707 (2016).

[16] Y. Yamaguchi, T. Nakano, Y. Nozue, and T. Kimura, Magnetoelectric effect in an *XY*-like spin glass system $Ni_xMn_{1-x}TiO_3$, Phys. Rev. Lett. **108**, 057203 (2012).

[17] S. Sharma, T. Basu, A. Shahee, K. Singh, N. P. Lalla, and E. V. Sampathkumaran, Multiglass properties and magnetoelectric coupling in the uniaxial anisotropic spin-cluster-glass Fe_2TiO_5, Phys. Rev. B **90**, 144426 (2014).

[18] W. Kleemann, V. V. Shvartsman, P. Borisov, and A. Kania, Coexistence of antiferromagnetic and spin cluster glass order in the magnetoelectric relaxor multiferroic $PbFe_{0.5}Nb_{0.5}O_3$, Phys. Rev. Lett. **105**, 257202 (2010).

[19] E. Maniv, R. A. Murphy, S. C. Haley, S. Doyle, C. John, A. Maniv, S. K. Ramakrishna, Y.-L. Tang, P. Ercius, R. Ramesh *et al.*, Exchange bias due to coupling between coexisting antiferromagnetic and spin-glass orders, Nat. Phys. **17**, 525 (2021).

[20] J. A. Mydosh, *Spin Glasses: An Experimental Introduction* (Taylor & Francis, London, 1993).

[21] M. Ali, P. Adie, C. H. Marrows, D. Greig, B. J. Hickey, and R. L. Stamps, Exchange bias using a spin glass, Nat. Mater. **6**, 70 (2007).

[22] M. Ali, C. H. Marrows, and B. J. Hickey, Controlled enhancement or suppression of exchange biasing using impurity δ layers, Phys. Rev. B **77**, 134401 (2008).

[23] J. F. Ding, O. I. Lebedev, S. Turner, Y. F. Tian, W. J. Hu, J. W. Seo, C. Panagopoulos, W. Prellier, G. Van Tendeloo, and T. Wu, Interfacial spin glass state and exchange bias in manganite bilayers with competing magnetic orders, Phys. Rev. B **87**, 054428 (2013).

[24] T. Kurumaji, S. Ishiwata, and Y. Tokura, Diagonal magnetoelectric susceptibility and effect of Fe doping in the polar ferrimagnet $Mn_2Mo_3O_8$, Phys. Rev. B **95**, 045142 (2017).

[25] Y. Wang, G. L. Pascut, B. Gao, T. A. Tyson, K. Haule, V. Kiryukhin, and S.-W. Cheong, Unveiling hidden ferrimagnetism and giant magnetoelectricity in polar magnet $Fe_2Mo_3O_8$, Sci. Rep. **5**, 12268 (2015).

[26] Y. S. Tang, G. Z. Zhou, L. Lin, R. Chen, J. F. Wang, C. L. Lu, L. Huang, J. H. Zhang, Z. B. Yan, X. M. Lu *et al.*, Successive electric polarization transitions induced by high magnetic field in the single-crystal antiferromagnet $Co_2Mo_3O_8$, Phys. Rev. B **105**, 064108 (2022).

[27] Y. S. Tang, J. H. Zhang, L. Lin, R. Chen, J. F. Wang, S. H. Zheng, C. Li, Y. Y. Zhang, G. Z. Zhou, L. Huang *et al.*, Metamagnetic transitions and magnetoelectricity in the spin-1 honeycomb antiferromagnet $Ni_2Mo_3O_8$, Phys. Rev. B **103**, 014112 (2021).

[28] Z. Yu, H. Ding, K. Zhai, C. Mu, A. Nie, J. Cong, J. Huang, H. Zhou, Q. Wang, F. Wen, J. Xiang *et al.*, Crystal structure, spin flop transition, and magnetoelectric effect in the honeycomb-lattice frustrated Fe-doped $Ni_2Mo_3O_8$ antiferromagnets, Phys. Rev. B **109**, 024442 (2024).

[29] W. H. McCarroll, L. Katz, and R. Ward, Some ternary oxides of tetravalent molybdenum[1,2], J. Am. Chem. Soc. **79**, 5410 (1957).

[30] J. K. Yang, D. Su, J. C. He, Y. Ji, Q. W. Guo, Y. Meng, X. F. Li, L. Y. Wang, X. Shen, Y. Yao *et al.*, Mg doping enhanced magnetoelectric effect in the polar magnet $Fe_2Mo_3O_8$, Phys. Rev. B **107**, 104408 (2023).

[31] S. K. Yu, B. Gao, J. W. Kim, S.-W. Cheong, M. K. L. Man, J. Madéo, K. M. Dani, and D. Talbayev, High-temperature terahertz optical diode effect without magnetic order in polar $FeZnMo_3O_8$, Phys. Rev. Lett. **120**, 037601 (2018).

[32] T. N. Stanislavchuk, G. L. Pascut, A. P. Litvinchuk, Z. Liu, S. Choi, M. J. Gutmann, B. Gao, K. Haule, V. Kiryukhin, S.-W. Cheong *et al.*, Spectroscopic and first principle DFT + eDMFT study of complex structural, electronic, and vibrational properties of $M_2Mo_3O_8$ (M = Fe, Mn) polar magnets, Phys. Rev. B **102**, 115139 (2020).

[33] P. Strobel, Y. Le Page, and S. P. McAlister, Growth and physical properties of single crystals of $Fe_2^{II}Mo_3^{IV}O_8$, J. Solid State Chem. **42**, 242 (1982).

[34] G. M. Sheldrick, Crystal structure refinement with SHELXL, Acta Crystallogr. Sect. C **71**, 3 (2015).

[35] K. Ishizuka, Prospects of atomic resolution imaging with an aberration–corrected STEM, J. Electron Microsc. (Tokyo) **50**, 291 (2001).

[36] See Supplemental Material at http://link.aps.org/supplemental/10.1103/yn33-jfp3 for the doping ratios in different regions of sample; the SAED pattern of $FeNiMo_3O_8$ (FNMO); data collection and structure refinement of FNMO; positions of atoms in FNMO; HAADF simulation images for two structural models; SAED patterns of FNMO at 293 and 95 K; variation of lattice constants with temperature; the Curie-Weiss fitting results along the c-axis and a-axis; pyroelectricity of FNMO; calculation of ligand field stabilization energy; and variations of dc susceptibility with temperature.

[37] F. Varret, H. Czeskleba, F. Hartmann-Boutron, and P. Imbert, Étude par effet Mössbauer de l'ion Fe^{2+} en symétrie trigonale dans les composés du type $(Fe, M)_2Mo_3O_8$ (M = Mg, Zn, Mn, Co, Ni) et propriétés magnétiques de $(Fe, Zn)_2Mo_3O_8$, J. Phys. **33**, 549 (1972).

[38] J. R. Morey, A. Scheie, J. P. Sheckelton, C. M. Brown, and T. M. McQueen, $Ni_2Mo_3O_8$: Complex antiferromagnetic order on a honeycomb lattice, Phys. Rev. Mater. **3**, 014410 (2019).

[39] P. Müller, R. Herbst-Irmer, A. L. Spek, T. R. Schneider, and M. R. Sawaya, *Crystal Structure Refinement: A Crystallographer's Guide to SHELXL* (Oxford University Press, Oxford, 2006).

[40] S. J. Pennycook, S. D. Berger, and R. J. Culbertson, Elemental mapping with elastically scattered electrons, J. Microsc. **144**, 229 (1986).

[41] M. M. J. Treacy, Z dependence of electron scattering by single atoms into annular dark-field detectors, Microsc. Microanal. **17**, 847 (2011).

[42] S. Reschke, A. A. Tsirlin, N. Khan, L. Prodan, V. Tsurkan, I. Kézsmárki, and J. Deisenhofer, Structure, phonons, and orbital degrees of freedom in $Fe_2Mo_3O_8$, Phys. Rev. B **102**, 094307 (2020).

[43] D. I. Khomskii and S. V. Streltsov, Orbital effects in solids: Basics, recent progress, and opportunities, Chem. Rev. **121**, 2992 (2021).

[44] D. I. Khomskii, T. Mizokawa, and S. V. Streltsov, Comment on "Spin-lattice coupling and the emergence of the trimerized phase in the $S = 1$ kagome antiferromagnet $Na_2Ti_3Cl_8$, Phys. Rev. Lett. **127**, 049701 (2021).

[45] G. L. Miessler, P. J. Fischer, and D. A. Tarr, *Inorganic Chemistry*, 5th ed. (Pearson, Boston, 2014).

[46] J. A. Mydosh, Spin glasses: Redux: An updated experimental/materials survey, Rep. Prog. Phys. **78**, 052501 (2015).

[47] S. Bedanta and W. Kleemann, Supermagnetism, J. Phys. Appl. Phys. **42**, 013001 (2008).

[48] M. Viswanathan and P. S. A. Kumar, Observation of reentrant spin glass behavior in $LaCo_{0.5}Ni_{0.5}O_3$, Phys. Rev. B **80**, 012410 (2009).

[49] P. C. Hohenberg and B. I. Halperin, Theory of dynamic critical phenomena, Rev. Mod. Phys. **49**, 435 (1977).

[50] J. Souletie and J. L. Tholence, Critical slowing down in spin glasses and other glasses: Fulcher versus power law, Phys. Rev. B **32**, 516 (1985).

[51] S. Ghara, B.-G. Jeon, K. Yoo, K. H. Kim, and A. Sundaresan, Reentrant spin-glass state and magnetodielectric effect in the spiral magnet $BiMnFe_2O_6$, Phys. Rev. B **90**, 024413 (2014).

[52] A. Pal, P. Singh, V. K. Gangwar, S. Ghosh, P. Prakash, S. K. Saha, A. Das, M. Kumar, A. K. Ghosh, and S. Chatterjee, B-site disorder driven multiple-magnetic phases: Griffiths phase, re-entrant cluster glass, and exchange bias in Pr_2CoFeO_6, Appl. Phys. Lett. **114**, 252403 (2019).

[53] C. Djurberg, P. Svedlindh, P. Nordblad, M. F. Hansen, F. Bødker, and S. Mørup, Dynamics of an interacting particle system: Evidence of critical slowing down, Phys. Rev. Lett. **79**, 5154 (1997).

[54] K. Binder and W. Kob, *Glassy Materials and Disordered Solids: An Introduction to Their Statistical Mechanics* (World Scientific, Singapore, 2011).

[55] A. Ito, H. Aruga, E. Torikai, M. Kikuchi, Y. Syono, and H. Takei, Time-dependent phenomena in a short-range ising spin-glass, $Fe_{0.5}Mn_{0.5}TiO_3$, Phys. Rev. Lett. **57**, 483 (1986).

[56] P. D. Mitchler, R. M. Roshko, and W. Ruan, Non-equilibrium relaxation dynamics in the spin glass and ferromagnetic phases of CrFe, Philos. Mag. B **68**, 539 (1993).

[57] J. Nogués and I. K. Schuller, Exchange bias, J. Magn. Magn. Mater. **192**, 203 (1999).

[58] M. Kiwi, Exchange bias theory, J. Magn. Magn. Mater. **234**, 584 (2001).

[59] X. Wang, Y. S. Chai, L. Zhou, H. B. Cao, C.-D. Cruz, J. Y. Yang, J. H. Dai, Y. Y. Yin, Z. Yuan, S. J. Zhang *et al.*, Observation of magnetoelectric multiferroicity in a cubic perovskite system: $LaMn_3Cr_4O_{12}$, Phys. Rev. Lett. **115**, 087601 (2015).

[60] X. D. Shen, L. Zhou, Y. S. Chai, Y. Wu, Z. H. Liu, Y. Y. Yin, H. B. Cao, C. De la Cruz, Y. Sun, C. Q. Jin *et al.*, Large linear magnetoelectric effect and field-induced ferromagnetism and ferroelectricity in $DyCrO_4$, NPG Asia Mater. **11**, 50 (2019).

[61] Y. Kohara, Y. Yamasaki, Y. Onose, and Y. Tokura, Excess-electron induced polarization and magnetoelectric effect in yttrium iron garnet, Phys. Rev. B **82**, 104419 (2010).

[62] C. De, S. Ghara, and A. Sundaresan, Effect of internal electric field on ferroelectric polarization in multiferroic $TbMnO_3$, Solid State Commun. **205**, 61 (2015).

[63] X. Wang, F.-T. Huang, J. Yang, Y. S. Oh, and S.-W. Cheong, Interlocked chiral/polar domain walls and large optical rotation in Ni_3TeO_6, APL Mater. **3**, 076105 (2015).

[64] R. D. Johnson, K. Cao, F. Giustino, and P. G. Radaelli, $CaBaCo_4O_7$: A ferrimagnetic pyroelectric, Phys. Rev. B **90**, 045129 (2014).

[65] T. Kurumaji, S. Ishiwata, and Y. Tokura, Doping-tunable ferrimagnetic phase with large linear magnetoelectric effect in a polar magnet $Fe_2Mo_3O_8$, Phys. Rev. X **5**, 031034 (2015).

[66] Z. Z. Kong, C. J. Kaminsky, C. K. Groschner, R. A. Murphy, Y. Yu, S. Husremovic, L. L. S. Xie, M. P. Erodici, R. S. Kim, J. Yano *et al.*, Near room-temperature intrinsic exchange bias in an fe intercalated $ZrSe_2$ spin glass, J. Am. Chem. Soc. **145**, 20041 (2023).

[67] R. G. Burns and W. S. Fyfe, Site of preference energy and selective uptake of transition-metal ions from a magma, Science **144**, 1001 (1964).

[68] M. Gruyters, Spin-glass-like behavior in CoO nanoparticles and the origin of exchange bias in layered CoO/Ferromagnet structures, Phys. Rev. Lett. **95**, 077204 (2005).

[69] G. Parisi, Order parameter for spin-glasses, Phys. Rev. Lett. **50**, 1946 (1983).

[70] K. Binder and A. P. Young, Spin glasses: Experimental facts, theoretical concepts, and open questions, Rev. Mod. Phys. **58**, 801 (1986).

[71] A. V. Semeno, M. A. Anisimov, A. V. Bogach, S. V. Demishev, M. I. Gilmanov, V. B. Filipov, N. Y. Shitsevalova, and V. V. Glushkov, Role of spin-glass behavior in the formation of exotic magnetic states in GdB6, Sci. Rep. **10**, 18214 (2020).

[72] Y. Liu, J. J. Bao, C. Q. Xu, W. H. Jiao, H. Zhang, L. C. Xu, Z. W. Zhu, H. Y. Yang, Y. H. Zhou, Z. Ren *et al.*, Coupling between antiferromagnetic and spin-glass orders in the quasi-one-dimensional iron telluride $TaFe_{1+x}Te_3$ ($x = 0.25$), Phys. Rev. B **104**, 104418 (2021).

[73] W. H. Meiklejohn and C. P. Bean, New magnetic anisotropy, Phys. Rev. **105**, 904 (1957).

[74] B. M. Wang, Y. Liu, P. Ren, B. Xia, K. B. Ruan, J. B. Yi, J. Ding, X. G. Li, and L. Wang, Large exchange bias after zero-field cooling from an unmagnetized state, Phys. Rev. Lett. **106**, 077203 (2011).

[75] J. Krishna Murthy and A. Venimadhav, Giant zero field cooled spontaneous exchange bias effect in phase separated $La_{1.5}Sr_{0.5}CoMnO_6$, Appl. Phys. Lett. **103**, 252410 (2013).

[76] L. T. Coutrim, E. M. Bittar, F. Stavale, F. Garcia, E. Baggio-Saitovitch, M. Abbate, R. J. O. Mossanek, H. P. Martins, D. Tobia, P. G. Pagliuso *et al.*, Compensation temperatures and exchange bias in $La_{1.5}Ca_{0.5}CoIrO_6$, Phys. Rev. B **93**, 174406 (2016).

[77] L. T. Coutrim, E. M. Bittar, F. Garcia, and L. Bufaiçal, Influence of spin glass-like magnetic relaxation on the zero-field-cooled exchange bias effect, Phys. Rev. B **98**, 064426 (2018).

[78] V. V. Shvartsman, S. Bedanta, P. Borisov, W. Kleemann, A. Tkach, and P. M. Vilarinho, (Sr, Mn)TiO_3: A magnetoelectric multiglass, Phys. Rev. Lett. **101**, 165704 (2008).

[79] S. Dong, H. Xiang, and E. Dagotto, Magnetoelectricity in multiferroics: A theoretical perspective, Natl. Sci. Rev. **6**, 629 (2019).